Cerebral Cortex, 2020;00: 1–15

doi: 10.1093/cercor/bhz191
Original Article

ORIGINAL ARTICLE

Disruption of Transient SERT Expression in Thalamic Glutamatergic Neurons Alters Trajectory of Postnatal Interneuron Development in the Mouse Cortex

Roberto De Gregorio[1], Xiaoning Chen[1], Emilie I. Petit[1], Kostantin Dobrenis[2] and Ji Ying Sze[1]

[1]Department of Molecular Pharmacology, Albert Einstein College of Medicine, The Bronx, NY 10461, USA and [2]Dominick P. Purpura Department of Neuroscience, Albert Einstein College of Medicine, The Bronx, NY 10461, USA

Address correspondence to Ji Ying Sze, Department of Molecular Pharmacology, Albert Einstein College of Medicine, The Bronx, NY 10461, USA. Email: jiying.sze@einstein.yu.edu.

Abstract

In mice, terminal differentiation of subpopulations of interneurons occurs in late postnatal stages, paralleling the emergence of the adult cortical architecture. Here, we investigated the effects of altered initial cortical architecture on later interneuron development. We identified that a class of somatostatin (SOM)-expressing GABAergic interneurons undergoes terminal differentiation between 2nd and 3rd postnatal week in the mouse somatosensory barrel cortex and upregulates Reelin expression during neurite outgrowth. Our previous work demonstrated that transient expression (E15-P10) of serotonin uptake transporter (SERT) in thalamocortical projection neurons regulates barrel elaboration during cortical map establishment. We show here that in thalamic neuron SERT knockout mice, these SOM-expressing interneurons develop at the right time, reach correct positions and express correct neurochemical markers, but only 70% of the neurons remain in the adult barrel cortex. Moreover, those neurons that remain display altered dendritic patterning. Our data indicate that a precise architecture at the cortical destination is not essential for specifying late-developing interneuron identities, their cortical deposition, and spatial organization, but dictates their number and dendritic structure ultimately integrated into the cortex. Our study illuminates how disruption of temporal-specific SERT function and related key regulators during cortical map establishment can alter interneuron development trajectory that persists to adult central nervous system.

Key words: cortical map architecture, dendrite patterning, postnatal interneuron development, temporal-specific SERT function

Introduction

Development of the cerebral cortex of the mammalian brain follows a highly stereotyped series of histogenic processes, during which an enormous variety of neuronal types are organized into functionally distinct areas with characteristic architecture, neuronal composition, and connectivity, forming the biological framework for perception, cognition, and behavior. Whereas the basic cortical maps are established by perinatal stages, neuronal differentiation processes continue well into childhood, with defined subpopulations of neurons sequentially recruited into existing circuits (Geschwind and Rakic 2013; Silbereis et al. 2016). In particular, in the mouse neocortex and hippocampus, terminal differentiation processes, such as cortical area assignment, laminar deposition, neurochemical identity and dendritic

arborization of diverse subtypes of GABAergic interneurons take place in late postnatal stages and even in adulthood (Wonders and Anderson 2006; Cossart 2011; Bartolini et al. 2013; Sultan et al. 2013). This extended postnatal expansion of neuronal populations is thought critical in shaping cognitive capacity and complex behavior (Stiles and Jernigan 2010; Lee et al. 2014; Silbereis et al. 2016). Indeed, disrupting the development of restricted GABAergic neuron subpopulations or subtle alterations of their functional properties may increase susceptibility to epilepsy, mental retardation, autism and schizophrenia (Cobos et al. 2005; Di Cristo 2007; Batista-Brito et al. 2008; de la Torre-Ubieta et al. 2016; Marin 2016). Recent advances in imaging, genetic, and genomic technologies have provided new insights into the diversity of interneuron types and their generation, migration, and distribution (Paul et al. 2017; Wamsley and Fishell 2017; Lim et al. 2018). However, genetic dissection of late developmental processes in the central nervous system (CNS) has been challenging. Despite the long-standing hypothesis for an interplay between cell-intrinsic and environmental signaling in interneuron terminal differentiation, little is known about the endogenous hierarchical processes that build brain region-specific architecture over a protracted period of time and how neurons that arrive in late postnatal stages are incorporated into existing cortical architecture (Rakic et al. 2009; Wamsley and Fishell 2017; Lim et al. 2018).

Mounting evidence suggests that pathological genetic variations and environmental insults affecting certain critical periods alter CNS developmental trajectory (de la Torre-Ubieta et al. 2016; Marin 2016; Silbereis et al. 2016). Transcriptome analysis with postmortem human brain samples revealed that biologically pleiotropic genes associated with neurodevelopmental and psychiatric disorders display temporal-specific cortical topographic expression during development (Chen et al. 2015a; Silbereis et al. 2016). To experimentally elucidate genetic programming of CNS architecture and how changes in early life may affect the adult CNS, it is helpful if both a gene function and affected neurons in specific brain regions at specific developmental stages can be monitored in real time, so that when and which processes affected can be delineated. Our previous work identified that transient early expression of serotonin (5-HT) uptake transporter (SERT) in glutamatergic thalamocortical projection neuron axons (TCA) regulates sensory map elaboration in mice (Chen et al. 2015b; Chen et al. 2016). Specifically, SERT is expressed from embryonic day 15 (E15) to postnatal day 10 (P10) in thalamic ventrobasal (VB) glutamatergic neurons projecting to the somatosensory barrel cortex (Hansson et al. 1998; Lebrand et al. 1998; Narboux-Neme et al. 2008). These neurons, termed "5-HT-absorbing neurons," do not synthesize 5-HT but take up trophic 5-HT from the extracellular space to prevent excessive 5-HT at their target brain regions (Lebrand et al. 1996; Chen et al. 2015b). Using the Cre/LoxP system to generate neuron-specific SERT knockout mice, we have shown that the barrel architecture is affected in TCA SERT knockout ($SERT^{Glu\Delta}$) mice (Chen et al. 2015b; Chen et al. 2016), providing a genetic paradigm for investigating how disrupting a gene function in TCA during cortical map establishment may influence later neuronal developmental processes in the cortex.

In the present study, we focused on a set of GABAergic interneurons developing in postnatal barrel cortex and characterized the effects of SERT disruption on their development using $SERT^{Glu\Delta}$ mice. Mouse lines expressing knock-in green fluorescent protein (GFP) reporter driven by promoter elements of the GABA synthesis enzyme glutamate decarboxylase 67 gene (GAD67-GFP) confer GFP expression in specific subpopulations of GABAergic neurons and have been used successfully in characterizing development and synaptic properties of reproducible subgroups of GABAergic neurons in the CNS (Oliva et al. 2000; Meyer et al. 2002; Chattopadhyaya et al. 2004; Ma et al. 2006; Gentet et al. 2012; Xu et al. 2013). Here, we show that the *GAD67-GFP/GIN* line (Oliva et al. 2000) expresses GFP in a population of somatostatin (SOM)-expressing GABAergic interneurons that develop in late postnatal barrel cortex. We demonstrate that defective barrel architecture in $SERT^{Glu\Delta}$ mice does not alter development timing of these interneurons, their deposition in barrels and their ability to express correct neurochemical identities, but has a profound impact on the number of the neurons that ultimately remain in the barrel cortex and their dendrite patterning, thereby linking SERT function in the TCA during initial cortical map establishment to cortical integration of interneurons in later developmental stages.

Materials and Methods

Animals

Animal use and procedures were approved by the Albert Einstein College of Medicine Institutional Animal Care and Use Committee. Generation of TCA SERT conditional knockout mice $SERT^{Glu\Delta}$ has been previously described (Chen et al. 2015b). Briefly, $SERT^{Glu\Delta}$ mice were generated by crossing $SERT^{fl/fl}$ mice, which carry LoxP sites flanking exons 3 and 4 of the SERT gene *Slc6a4*, and *Vglut2-Cre* mice, and Cre recombinase-mediated deletion results in a reading frameshift that eliminates SERT function (Chen et al. 2015b). *Vglut2-Cre* mice (Vong et al. 2011) were generated and generously shared by Bradford B. Lowell and colleagues. GAD67-GFP/GIN mice were generated by John W. Swann and colleagues (Oliva et al. 2000) and purchased from the Jackson Laboratories. All mouse strains have been backcrossed with C57B6 from Taconic Bioscience 9–11 times in our laboratory. To characterize the effects of disrupting TCA SERT expression on *GAD67-GFP/GIN*-expressing neurons, the GFP transgene was first crossed into $SERT^{fl/fl}$ to generate $SERT^{fl/fl}$;GFP/GFP mice, and $SERT^{fl/fl}$;GFP/GFP female mice were then crossed with $SERT^{fl/fl}$;*Vglut2-Cre*/+ ($SERT^{Glu\Delta}$) males to generate $SERT^{Glu\Delta}$;GFP/+ and no-Cre control $SERT^{fl/fl}$;GFP/+ mice for analysis. In this way, a larger number of progeny mice carried the same *Vglut2-Cre* transgene from a male, and all tested mice carried one copy of *GAD67-GFP/GIN* transgene. For every experiment throughout this work, $SERT^{Glu\Delta}$;GFP/+ and control $SERT^{fl/fl}$;GFP/+ littermate mice were processed in parallel, with the genotype and sex of the mice blinded for the performers. Analysis of mutant and control littermates showed no appreciable sex-dependent differences, and consequently, male and female results were combined for presentation.

Immunohistochemistry and Histology

Mice were anesthetized by intraperitoneal injection of Avertin (400 mg/kg) prior to transcardial perfusion with phosphate-buffered saline (PBS) followed by 4% paraformaldehyde (PFA) in PBS, and brains were dissected. To obtain tangential sections of the barrel cortex, neocortical sheets were separated from the underlying white matter and flattened between two glass slides, postfixed overnight in 4% PFA and processed immediately. Flattened cortical sheets were sectioned tangentially to the pial surface in serial at 50 µm thickness, unless noted

otherwise, on a Vibratome (Leica). For immunostaining, sections were washed 3 × 10 min in PBS, 1 × 30 min in PBS with 0.3% Triton, and blocked with 5% donkey or goat serum and 0.1% Triton in PBS for 1 h at room temperature, before incubation with primary antibodies for 24–48 h at 4°C. For immunostaining of GABA, 0.2% of glutaraldehyde was added into fixative during perfusion and postfix, and the staining of brain sections was carried out without triton. For BrdU staining, sections were incubated in 2 N HCl for 1 h at room temperature and rinsed 3 × 5 min in PBS before applying the blocking solution. The following primary antibodies and dilutions were used: rat α-BrdU (1:500, Abcam AB6326), mouse α-calretinin (α-CR, 1:1000, Millipore MAB1568), rabbit α-CR (1:1000, Sigma C7479), guinea pig α-GABA (1:1000, Millipore AB175), rabbit α-GFP (1:1000, Invitrogen A6455), mouse α-GFP (1:1000, NeuroMab 75–132), chicken α-GFP (1:1000, Abcam AB13970), rabbit α-NPY (1:1000, Cell Signaling 11976S), mouse α-parvalbumin (PV, 1:1000, Sigma P3088), mouse α-Reelin (1:1000, Millipore MAB5364), rat α-somatostatin (1:30, Abcam AB30788), rat α-somatostatin (1:80, Abcam AB30788), guinea pig α-Vglut2 (1:1000, Millipore AB2251), and rabbit α- vasoactive intestinal peptide (1:500, Immunostar 20 077). Immunostaining of the proteins, BrdU and GABA was visualized by using secondary antibodies conjugated with fluorescent dye 488, 555, 568, or 647 at a dilution of 1:400. Donkey α-chicken 488 was purchased from Sigma (SAB460003), and the others were highly cross-absorbed secondary antibodies from Invitrogen. Sections were counterstained with 4′,6-diamidino-2-phenylindole (DAPI; Thermo Fisher D1306) to detect cell nuclei. Widefield microscopy fluorescence images were captured using an Axiocam MR digital camera attached to a Zeiss AxioImager Z1 microscope. Confocal images were collected using a laser point-scanning Zeiss LSM 880 Airyscan microscope. In this work, a defined set of nine barrels in arcs 1–3 of rows B–D of the posterior medial barrel subfields (PMBSF) was used as a model for analysis and comparisons between age groups and mutant and control mice.

For characterizing the morphology of *GAD67-GFP/GIN*-expressing neurons during postnatal development, serial 60 µm thick tangential sections through the barrel cortex of P7 and P12 pups were stained with anti-GFP antibody, and GFP+ neurons located in arcs 1–3 of rows B–D of the PMBSF were randomly selected for imaging. For each neuron, serial confocal images were taken along the Z-axis at 2.15 µm-interval. To visualize GFP+ neuron morphology, a maximum projection image was created from the image stack using FIJI software (ImageJ, NIH), encompassing optical planes 12 µm above and below the center of the cell body. In this study, GFP+ cells with thicker, multiple branched neurites are considered as mature morphological features, in contrast to simple round somas and thin short neurites of immature neurons.

For comparisons of Reelin immunoreactivity in *GAD67-GFP/GIN*-expressing neurons at various postnatal stages, brains collected from different age groups were processed in parallel. Serial 50 µm thick tangential sections through the barrel cortex were double immunostained for Reelin and GFP, and GFP+ neurons in arcs 1–3 of rows B–D of the PMBSF were randomly imaged using a 40X objective on a Zeiss AxioImager Z1 microscope, with fixed exposure time and camera gain. To quantify Reelin immunoreactivity, images were processed using FIJI to create regions of interest (ROI) around the somata of GFP+ cells, background fluorescence levels were determined in each image and subtracted, and ROI fluorescence intensity was quantified using FIJI.

Quantifying the Number of *GAD67-GFP/GIN*-Expressing Neurons in the Barrel Cortex

The number of *GAD67-GFP/GIN*-expressing neurons and their spatial distribution in the barrel cortex were determined by two methods. In all cases, serial tangential sections through the PMBSF were analyzed. GFP immunostaining was used to enhance visibility and DAPI was used as a counterstain of cell nuclei to delineate barrel boundaries. In the first method, barrel walls and hollows were defined as we have done previously (Chen et al. 2015b). Briefly, a barrel wall was defined as a ring of densely packed cell nuclei stained by DAPI, and the area surrounded by a barrel wall was defined as a barrel hollow. Images of DAPI staining were processed using mean filter and bandpass filter tools of ImageJ to obtain "smoothened" images (Supplementary Fig. S1A). By superimposing this image to the corresponding GFP image, the number of GFP+ cell bodies in barrel walls and hollows in arcs 1–3 of rows B–D of the PMBSF was quantified using the Cell Counter plugin, (ImageJ). The second method added Vglut2 immunostaining to label TCA in addition to GFP and DAPI staining, and images of Vglut2 staining were processed to define barrel walls and barrel hollows (Supplementary Fig. S1B), and the number of GFP+ cell bodies in barrel walls and hollows was quantified using the Cell Counter plugin. For each mouse, data represent the average of per 50 µm-thick section of serial sections through the nine-barrel area, unless noted otherwise.

To assess the time course of *GAD67-GFP/GIN*-expressing neurons arising, mice from the same litter at 2–3 ages were analyzed to detect changes over the ages, and mice from different litters were analyzed to account for variations between mice. To assess the time course of GFP+ neurons arising in the neocortex globally, serial sections were collected from flattened neocortical sheets at various postnatal ages, imaged at ×5 magnification and the cortical sheet on each section was reconstructed by manual alignment and stitching of the images. Cortical layer corresponding to the barrel cortex was identified using DAPI counterstain.

To estimate apoptosis in the barrel cortex, a TUNEL assay was performed using the ApopTag Red In Situ Apoptosis Detection Kit (Millipore S7165) with modification. Briefly, serial 35 µm tangential sections through the barrel cortex were collected from P18 and P30 mice and immunostained for GFP and Vglut2. Stained sections from mutant and control littermates were transferred to the same glass slides, dried at 55 °C for 5 min, further permeabilized in 0.5% triton in PBS at 85 °C for 20 min according to a published procedure (Deng et al. 2001), and processed TUNEL according to manufacturer's instructions. For every trial, sections of the hippocampus from P2 mice were processed in parallel, and the robust programmed cell death in P2 CA3 (Mosley et al. 2017) served an additional positive control for the TUNEL assay. A total number of TUNEL+ cells in arcs 1–3 of rows B–D in serial sections of the PMBSF was quantified using the Cell Counter plugin, (ImageJ). Localization of TUNEL in GFP+ cell bodies was determined by confocal microscopy.

BrdU labeling was used to assess the birth of *GAD67-GFP/GIN*-expressing neurons located in the barrel cortex. The conception day was determined based on vaginal plug marks, and the following day was taken as E1.5. The date of birth of the pups was considered as P0. To mark embryonic neurogenesis, a single pulse of BrdU (MP Biomedicals 100 171) was administrated intraperitoneally into dams at 25 µg/g body weight at the pregnant stage of E10.5, E12.5, E13.5, E14.5, or E16.5. To label

neurons generated postnatally, BrdU was injected into pups at 100 µg/g body weight daily from P0 to P3, P3 to P10, or P10 to P16. To visualize BrdU labeling, 50 µm-thick serial tangential sections through the barrel cortex were collected from P16 mice that had been exposed to BrdU embryonically or postnatally and stained with anti-BrdU and anti-GFP antibodies. BrdU labeling at E10.5 was analyzed in four mice resulted from one injected dam, and for all other time points, four to eight mice from two independent litters were analyzed, and data are presented as mean ± standard error of the mean (SEM).

Dendrite Reconstructions and Analysis

Dendrite reconstructions and analyses were performed using similar criteria as described previously (Chen *et al.* 2015b). Briefly, 60 µm thick tangential sections through the PMBSF of P30 mice were stained with anti-GFP antibody, and DAPI was used as a cell nuclear counterstain for determining barrel boundaries in the PMBSF as described above. GFP+ neurons located close to the edge of barrel walls were randomly selected for imaging and analysis. For each neuron, serial confocal images were taken along the Z-axis at 1 µm intervals using a 40X objective. To analyze the dendritic architecture of the GFP+ neurons, a maximum projection image was created from an image stack, encompassing 20 µm above and below the center of the cell body. The dendritic trees were reconstructed using FIJI software. This image was superimposed over a DAPI-staining image taken at lower magnification to locate the position of the dendrites relative to barrel structures. Total dendritic length, branching points, and segments were quantified using NeuronJ. To evaluate dendritic orientation, a line crossing the center of the cell body was drawn in parallel to the barrel wall as described previously (Espinosa et al. 2009; Chen *et al.* 2015b). A barrel housing the majority of dendrite length of a GFP+ neuron was considered as the primary barrel, and dendritic profiles leading toward and/or located within the primary barrel were quantified.

Statistical Analyses

Statistical analyses were performed with GraphPad Prism. Data are presented as mean ± standard error of the mean (SEM). For all comparisons between $SERT^{Glu\Delta}$ and control mice, *P* values are based on two-tail, unpaired *t*-tests. For comparisons of the number of GFP-expressing neurons and Reelin immunoreactivity in the same genotype background at different postnatal ages, *P* values are based on repeated measure one-way ANOVA followed by Tukey post hoc tests. Differences were considered significant when the *P* value < 0.05.

Results

GAD67-GFP/GIN-Expressing Neurons Develop in Late Postnatal Somatosensory Barrel Cortex

To study late postnatal development, we sought to examine subpopulations of interneurons that undergo terminal differentiation in the mouse brain after the initial barrel structure is established. We were motivated by elegant work showing developmental onset of two waves of SOM-expressing interneurons in the rat neocortex and hippocampus: the first wave SOM neurons emerge at E16 reaching a plateau at P1 and the second wave SOM neurons arise between P9 and P15 and progressively deposit in discrete cortical layers and hippocampal subdivisions (Naus et al. 1988a; Naus et al. 1988b). Because in the brain SOM neurons are exclusively GABAergic (Urban-Ciecko and Barth 2016), we examined three transgenic mouse lines that are known expressing GAD67-GFP in subpopulations of SOM-expressing GABAergic neurons (Oliva et al. 2000; Ma et al. 2006) at a series of developmental stages. We found that the timing of *GAD67-GFP/GIN*-expressing neurons (Oliva et al. 2000) arising in the cortex closely matches the reported timing of the second wave SOM-expressing interneurons.

Supplementary Fig. S2 shows *GAD67-GFP/GIN*-expressing cells in the neocortex at various postnatal stages. GFP+ cells can first be detected approximately at P5, sparsely populated in caudal regions of the neocortex, and during the next 2 weeks GFP+ cells increased in number and spread throughout the cortex. To characterize development of the GFP-expressing cells, we made use of the exquisite somatotopic map in the PMBSF of the somatosensory cortex, where TCA form five rows of precisely arrayed patches representing individual whiskers; each TCA patch is surrounded by a wall of layer IV glutamatergic and GABAergic cortical neurons with each cortical neuron located in the wall sending dendrites into a single TCA patch to form a discrete anatomical unit—a barrel (Inan and Crair 2007). Since the barrels are established during the first postnatal week, we characterized GFP+ cells in the PMBSF at five time points from P7 to P45, with a focus on a defined set of nine barrels in arcs 1–3 of rows B–D (Fig. 1). At P7, only a few GFP+ cells were visible. Many GFP+ cells displayed characteristics for various early morphological developmental stages, with simple round somas and thin, short neurites (Figs 1B_1,$B_{2)}$. About 60% of GFP+ cells at P7 displayed somewhat mature morphological features such as thicker and multiple primary neurites sometimes branched (Figs 1B_1,B_2, and E). The number of GFP+ cells in the barrel cortex increased progressively in the next 10 days of life and their processes grew longer and more complex. At P12, more than 85% of GFP+ cells displayed mature morphological features, while there were few GFP+ cells at early morphological developmental stages (Fig. 1C_1,C_2, and E). These observations are in line with the report that *GAD67-GFP/GIN*-expressing neurons represent a population of SOM-expressing GABAergic neurons that initiate terminal differentiation around P5 in the hippocampus (Oliva et al. 2000).

Although postnatal origins of cortical interneurons exist, it is believed that most GABAergic neurons are born embryonically but some of them migrate and reach their final destination at postnatal stages (Wonders and Anderson 2006; Cossart 2011; Bartolini et al. 2013). To assess the time window of *GAD67-GFP/GIN*-expressing neuron birth, pregnant female mice at five time points of gestation from E10.5 to E16.5 and pups at three age groups from P0 to P16 were pulse labeled with BrdU, and brains from the resulting mice were collected at P16, the age when the number of GFP+ cells in the barrel cortex approaching a plateau (Fig. 1D). Double immunostaining showed 4.1 ± 2.7%, 16.1 ± 2.1%, 28.8 ± 5.1%, and 25.4 ± 2.6% of GFP+ cells in the barrel cortex were labeled by BrdU administrated at E10.5, E12.5, E13.5, and E14.5, respectively (Fig. 2). In contrast, exposure to BrdU at E16.5, or postnatally at P0–P3, P3–P10, and P10–P16 daily resulted in many BrdU-labeled cells but none of these were GFP+ (Fig. 2C). Combined, these data indicate that *GAD67-GFP/GIN*-expressing neurons were born predominantly around E13.5–14.5, but complete their terminal differentiation in the barrel cortex between the 2nd and 3rd postnatal week, after the somatotopic map has been established.

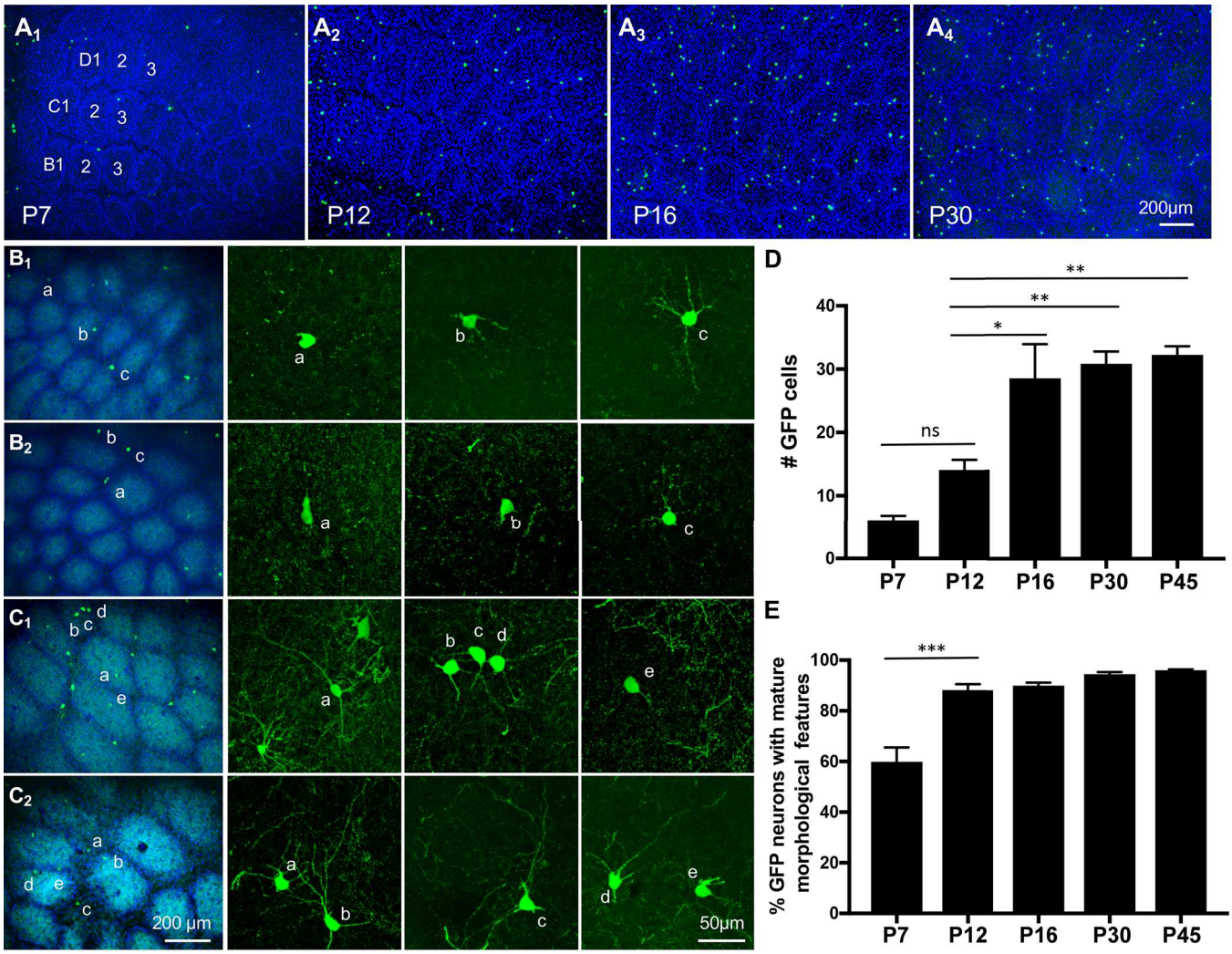

Figure 1. *GAD67-GFP/GIN*-expressing neurons arise and mature in the somatosensory barrel cortex at late postnatal stages. (*A*) Images of GFP-expressing neurons in tangential sections of the PMBSF at indicated ages. Barrels in arcs 1–3 of rows *B-D* are indicated in the image of P7 PMBSF. Noticing preferential localization of GFP+ cell bodies (green) in barrel walls outlined by densely packed DAPI-labeled nuclei (blue). Timing of GFP+ cells arising in the entire neocortical sheet is presented in Supplementary Fig. S2. (*B-C*) Representative images of GFP+ cell morphology at P7 (B_1, B_2) and P12 (C_1, C_2). The first column from the left shows low-magnification images of GFP+ neurons (green) in the PMBSF overlay with Vglut2-immunolabeled TCA (cyan) and DAPI counterstain of cell nuclei (blue), and neurons marked by letters are shown in confocal images in corresponding right panels. Neurons with simple morphology as displayed by neurons a in B_1, *a*, *b* in B_2, and *e* in C_1 are considered immature neurons, while longer and more complex neurites shown by the other neurons are considered as mature morphological features. (*D-E*) Quantification of the number of GFP+ cells in nine barrels in arcs 1–3 of rows *B-D* in PMBSF (*D*), and the fraction of the neurons displaying mature morphological features at indicated ages (*E*). GFP+ neurons in serial tangential sections through the PMBSF were analyzed, and data represent mean per 50 μm section ± SEM, N ≥ 3 mice for each age group. $^{*}P < 0.05$, $^{**}P < 0.01$, $^{***}P < 0.001$, and one-way ANOVA followed by Tukey post hoc tests.

GAD67-GFP/GIN-Expressing Cells Represent a Distinct Subset of SOM-Expressing GABAergic Neurons

Our immunostaining showed that *GAD67-GFP/GIN*-expressing neurons in the barrel cortex are GABAergic and SOM-expressing neurons (Figs 3A,B; Supplementary Fig. S3), consistent with previous reports (Oliva et al. 2000; Ma et al. 2006). Because multiple classes of GABAergic neurons expressing distinct chemical and molecular characteristics are localized to the barrel cortex, we asked if the GFP-expressing neurons represent a particular class of GABAergic neurons by double immunostaining of the barrel cortex from one-month-old mice with GFP and a series of established markers for GABAergic neuron subtypes.

We first determined that GFP+ neurons do not express markers for two other major classes of GABAergic neurons: parvalbumin (PV) and vasoactive intestinal peptide (VIP) (Wamsley and Fishell 2017). We observed many neurons in the barrel cortex displayed immunoreactivity for PV and VIP; however, neither PV nor VIP was detected in GFP+ neurons (Figs 3C,D; Supplementary Fig. S3; Table 1). Thus, the GFP was selectively expressed in SOM-expressing neurons.

Although all GFP+ neurons were immunoreactive for SOM (Fig. 3B, Supplementary Fig. S3; Table 1), only 32.1 ± 0.8% of SOM-immunolabeled neurons in the barrel cortex expressed GFP ($N = 3$ mice). Since SOM-expressing neurons comprise several subtypes by expressing other neurochemical markers, such

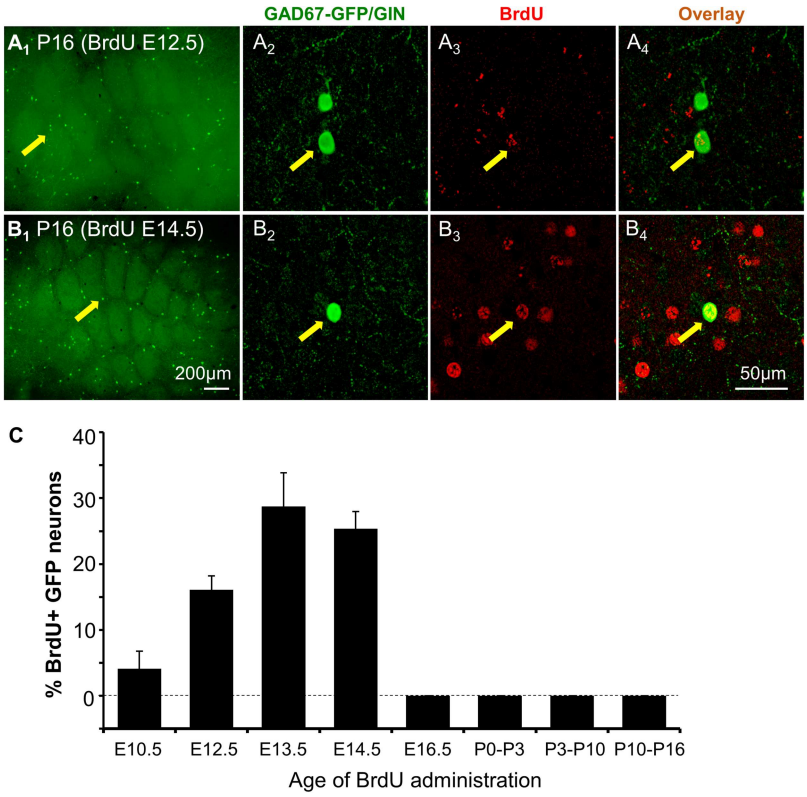

Figure 2. Barrel cortex *GAD67-GFP/GIN*-expressing neurons are born predominantly around E13.5 and E14.5 in mice. (*A*-*B*) Representative images of BrdU and GFP double immunostaining of tangential sections through the PMBSF from P16 mice exposed to BrdU at E12.5 (*A*) or E14.5 (*B*). A_2–A_4 and B_2–B_4 show confocal images of BrdU and GFP colocalization in neurons indicated by arrows in A_1 and B_1, respectively. (*C*) Quantification of the percentage of GFP+ neurons immunolabeled by BrdU over the total numbers of GFP+ neurons located in arcs 1–3 of rows *B*-*D* of the PMBSF from P16 mice exposed to BrdU at indicated ages. Error bars represent SEM, $N = 4$–8 mice per time point.

as the neuropeptide Y (NPY) and calcium-binding protein calretinin (CR) (Xu et al. 2006, 2010; Bartolini et al. 2013), we further characterized *GAD67-GFP/GIN*-expressing neuron identity by immunocolocalization of GFP with NPY or CR (Figs 3*E*,*F*; Supplementary Fig. S3). Only about 2% and 8% of GFP+ neurons showed immunoreactivity for NPY or CR, respectively (Supplementary Fig. S4; Table 1).

An earlier interesting work showed immunoreactivity for the extracellular matrix protein Reelin in about two-thirds of SOM-expressing GABAergic neurons in the primary somatosensory cortex of 3-week-old mice (Miyoshi et al. 2010), although less than 20% of SOM-expressing neurons display detectable Reelin in the adult primary somatosensory cortex (Alcantara et al. 1998). To determine if the GFP-expressing neurons represent a subpopulation of Reelin-expressing SOM neurons, we performed Reelin and GFP double immunostaining of the barrel cortex from P30 mice. We observed Reelin immunoreactivity in nearly all GFP+ neurons (Fig. 3*G*; Supplementary Fig. S3; Table 1). We further validated this observation by confirming colocalization of GFP+ neurons with both Reelin and SOM (Fig. 4*A*; Table 1). Quantification showed that GFP+ neurons constituted $34.5 \pm 2.6\%$ of total Reelin-immunolabeled cells in the barrel cortex ($N = 4$ mice). Since a small fraction of GFP+ cells expressed CR, we asked if Reelin is broadly expressed in CR-expressing neurons by triple immunostaining for CR, Reelin and GFP. We found that $8.2 \pm 3.2\%$ of CR+ neurons showed Reelin immunoreactivity, and all Reelin+/CR+ neurons were also GFP+ ($N = 3$ mice). Combined, these experiments indicate that the *GAD67-GFP/GIN*-expressing cells represent a subpopulation of SOM-expressing GABAergic neurons that express Reelin.

During rodent embryonic neurogenesis, Reelin expression coincides with the period of neurite outgrowth and synaptogenesis (Rakic and Caviness 1995; Alcantara *et al.* 1998). We wished to know if Reelin would also be dynamically expressed in postnatal developing neurons. We examined Reelin immunoreactivity in GFP+ neurons in the barrel cortex at five developmental time points where we monitored GFP-expressing neuron morphology (Fig. 4*B*). Quantification of the intensity of Reelin immunoreactivity in GFP+ cell bodies showed highest Reelin levels in GFP+ cells at P12 (Fig. 4*C*), corresponding to the timing of their robust neurite outgrowth (Fig. 1*E*), further indicating that *GAD67-GFP/GIN*-expressing cells in the barrel cortex elaborate cortical connectivity during late postnatal stages.

Genetic Dissection of *GAD67-GFP/GIN*-Expressing Neuron Development in $SERT^{Glu\Delta}$ Mice

A key question in determining hierarchical processes that build CNS functional architecture over a protracted period of time is the impact of initial cortical architecture on discrete developmental processes at subsequent stages. We noticed that *GAD67-GFP/GIN*-expressing neurons are preferentially localized to barrel walls (Fig. 1*A*), indicating that these neurons are integrated into the barrel structure. Since SERT expressed in TCA

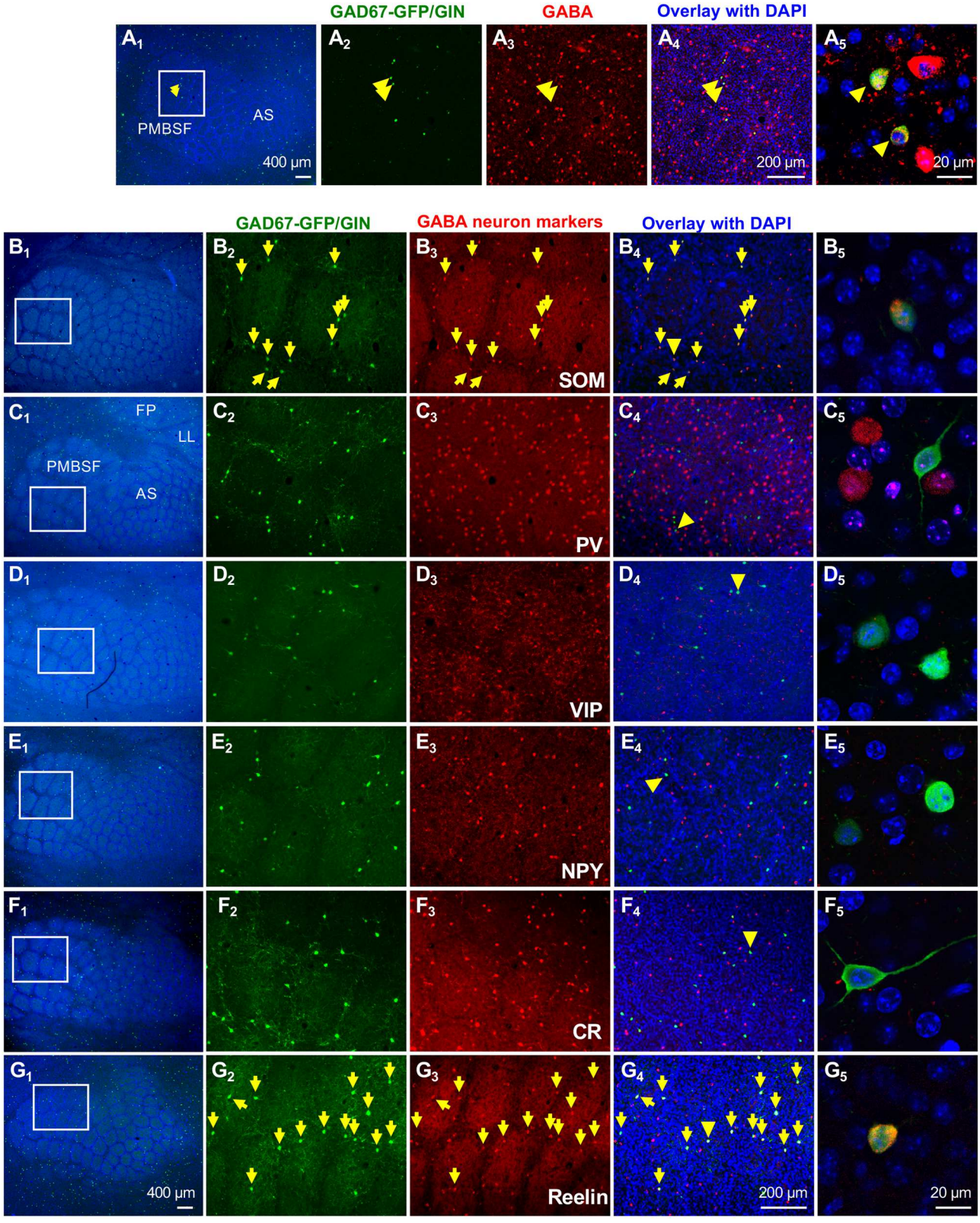

Figure 3. Barrel Cortex *GAD67-GFP/GIN*-expressing neurons represent a population of Reelin- and SOM-expressing GABAergic neurons. All images shown are tangential sections of the barrel cortex from P30 mice. (A) GFP and GABA double immunostaining. A_2–A_4 show GFP (green) and GABA (red) staining with DAPI counterstain (blue) in the PMBSF area outlined by a white box in A_1. A_5 shows a higher magnification confocal image of colocalization of GFP and GABA immunoreactivity in two neurons indicated by arrowheads. Noticing that GABA+ cell bodies display a ring patterning (barrel walls), and GFP+ neurons are preferentially localized to the ring. (*B*-*G*) Immunostaining for GFP and GABAergic neuron subtype markers. B_1–G_1 show low-magnification images of the barrel cortex with TCA immunolabeled by Vglut2 (cyan)

Table 1 Colocalization of GAD67-GFP/GIN with GABAergic neuron subtype markers in the barrel cortex[a]

	SOM/GFP	PV/GFP	VIP/GFP	CR/GFP	NPY/GFP	Reelin/GFP
Control	100 ± 0 (4)	0 ± 0 (4)	0 ± 0 (3)	8.1 ± 3.2(3)	1.6 ± 1.0(4)	99.7 ± 0.5(3)
SERTGluΔ	99.1 ± 1.1 (3)	0 ± 0 (3)	0 ± 0 (3)	6.5 ± 0.4(3)	2.6 ± 1.6(3)	97.6 ± 1.2(3)
P	0.42	–	–	0.69	0.62	0.22

[a]Percentages represent mean ± SEM of GFP+ cell bodies that are positive for immunostaining of indicated neuronal markers in serial tangential sections through the barrels in arcs 1–3 of rows B–D of the PMBSF in one-month-old mice. The number of animals analyzed for each staining is indicated in parenthesis. *P* values are based on unpaired *t*-tests.

regulates barrel formation during somatotopic map formation (Chen *et al.* 2015b), we, therefore, examined if and which steps of *GAD67-GFP/GIN*-expressing neuron development are altered in $SERT^{GluΔ}$ mice.

Immunostaining for SOM and the other markers showed that the neurochemical identities of *GAD67-GFP/GIN*-expressing neurons were not altered in $SERT^{GluΔ}$ mice (Supplementary Fig. S5; Table 1).

We next examined if the timing of *GAD67-GFP/GIN*-expressing neurons arising, their localization to and distribution in the barrel cortex would be altered in $SERT^{GluΔ}$ mice. Our previous studies showed that five rows of TCA patches in the PMBSF are preserved in $SERT^{GluΔ}$ mice, but the TCA patches are blurred because of poor segregation and patterning of layer IV neurons and their oriented dendritic arborization are lost (Chen *et al.* 2015b). We observed a few GFP+ neurons in the barrel cortex of P7 $SERT^{GluΔ}$ mice and the number increased by P16 as seen in control littermates (Fig. 5A), indicating that the general development timing of the GFP-expressing neurons was preserved in $SERT^{GluΔ}$ mice.

We further evaluated potential quantitative differences between $SERT^{GluΔ}$ and their control littermate mice by examining GFP+ neurons in the barrels in arcs 1–3 of rows B—D in the PMBSF. We found that the numbers of GFP+ neurons were comparable between $SERT^{GluΔ}$ and control littermate mice examined at P7, P10, P13, and P16, indicating that the number of the neurons successfully localized to the barrel cortex was unaffected (Fig. 5B). However, whereas in control mice the number of GFP+ neurons in the barrels at P30 and P62 stayed approximately the same as at P16, the number of GFP+ neurons became reduced in P30 and P62 $SERT^{GluΔ}$ barrels (Fig. 5B). On the other hand, the number of GFP+ neurons in the $SERT^{GluΔ}$ barrels at P62 was not significantly less than that at P30. Combined, these observations suggest that similar amounts of GFP-expressing neurons attained the barrel cortex at the peak around P16 in $SERT^{GluΔ}$ and control mice, but alterations in certain features caused by SERT deficit during initial barrel formation affected the number of the neurons able to remain in the cortex.

We asked whether $SERT^{GluΔ}$ alters spatial positioning of GFP+ neurons in the barrels, and, if so, is there a correlation between the spatial patterning and the change in the number of GFP+ neurons. We evaluated the spatial distribution of the GFP+ neurons by calculating the ratio of the number of GFP+ neurons in barrel walls relative to that in barrel hallows. In control mice at P7 through to P30, GFP+ neurons showed approximately a 2:1 ratio (Fig. 5C), matching the overall GABAergic neuron distribution in the barrel cortex (Chen *et al.* 2015b). While we could not appreciate a significant difference between $SERT^{GluΔ}$ and control mice at P7 and P10, ratios of GFP+ neurons in barrel walls versus that in barrel hollows in P13 and P16 $SERT^{GluΔ}$ mice were lower compared to that in control littermates, indicating an altered spatial distribution (Fig. 5C). Remarkably, the spatial distribution of GFP+ neurons in $SERT^{GluΔ}$ mice was comparable to that in control littermates at P30 (Fig. 5C).

It has long been appreciated that a surplus of neurons arriving in cortical regions is eliminated by programed cell death during assembly of cortical circuits (Raff et al. 1993; Voyvodic 1996; Lim et al. 2018). We thus considered the possibility that apoptosis was a cause for the reduced number of GFP+ neurons seen in P30 $SERT^{GluΔ}$ barrels, perhaps a similar number of the neurons arrived but less were able to integrate into the altered barrel structure. To test this possibility, we carried out TUNEL to visualize neuronal death in the barrel cortex. In serial tangential sections through the PMBSF of P18 and P30 mice, we observed TUNEL+ cells in both $SERT^{GluΔ}$ mice and control littermates (Fig. 5D). Consistent with the notion that apoptosis occurs to all classes of cortical neurons (Denaxa et al. 2018; Wong et al. 2018), most TUNEL+ cells displayed no appreciable GFP, while GFP was detectable in a few TUNEL+ cells (Fig. 5E). We also cannot exclude the possibility that GFP became undetectable in the late stages of dying cells. However, quantifying TUNEL+ cells in the barrels did not show a statistically significant change, although there was a trend of an increase in TUNEL+ cells in $SERT^{GluΔ}$ mice at P30 compared to that in control littermates (Fig. 5D).

Taken together, characterizations of *GAD67-GFP/GIN*-expressing neurons indicate that altered barrel architecture in $SERT^{GluΔ}$ mice did not impair the biological processes controlling features such as the neurochemical identity, their development timing, and localization to the barrel cortex. We hypothesize that the coincidental changes in spatial distribution and number of the GFP+ neurons in P30 $SERT^{GluΔ}$ barrels reflect a reduced number of the neurons able to incorporate into the existing sensory map.

and DAPI counterstain of the cell nuclei (blue). Receptive fields corresponding to specific body parts, whiskers (PMBSF), anterior snouts (AS), lower lip (LL), and forepaw (FP) are indicated in C_1. Higher magnification images of staining of GFP, indicated markers and overlay with DAPI in the regions outlined by white boxes are shown in B_2, B_3, and B_4–G_2, G_3, and G_4, respectively. Neurons stained by both GFP and indicated markers are pointed by yellow arrows. Confocal images of GFP+ neurons indicated by yellow arrowheads in B_4–G_4 are shown in B_5–G_5, and single-channel confocal images for individual staining of these neurons are presented in Supplementary Fig. S3. SOM and Reelin immunoreactivities were detectable in nearly all GFP+ cell bodies in the barrel cortex. No GFP+ neuron showed immunoreactivity for PV or VIP. Rarely, GFP+ neurons showed colocalization with NPY or CR (Supplementary Fig. S4). Quantification of colocalization of GFP with each marker is presented in Table 1.

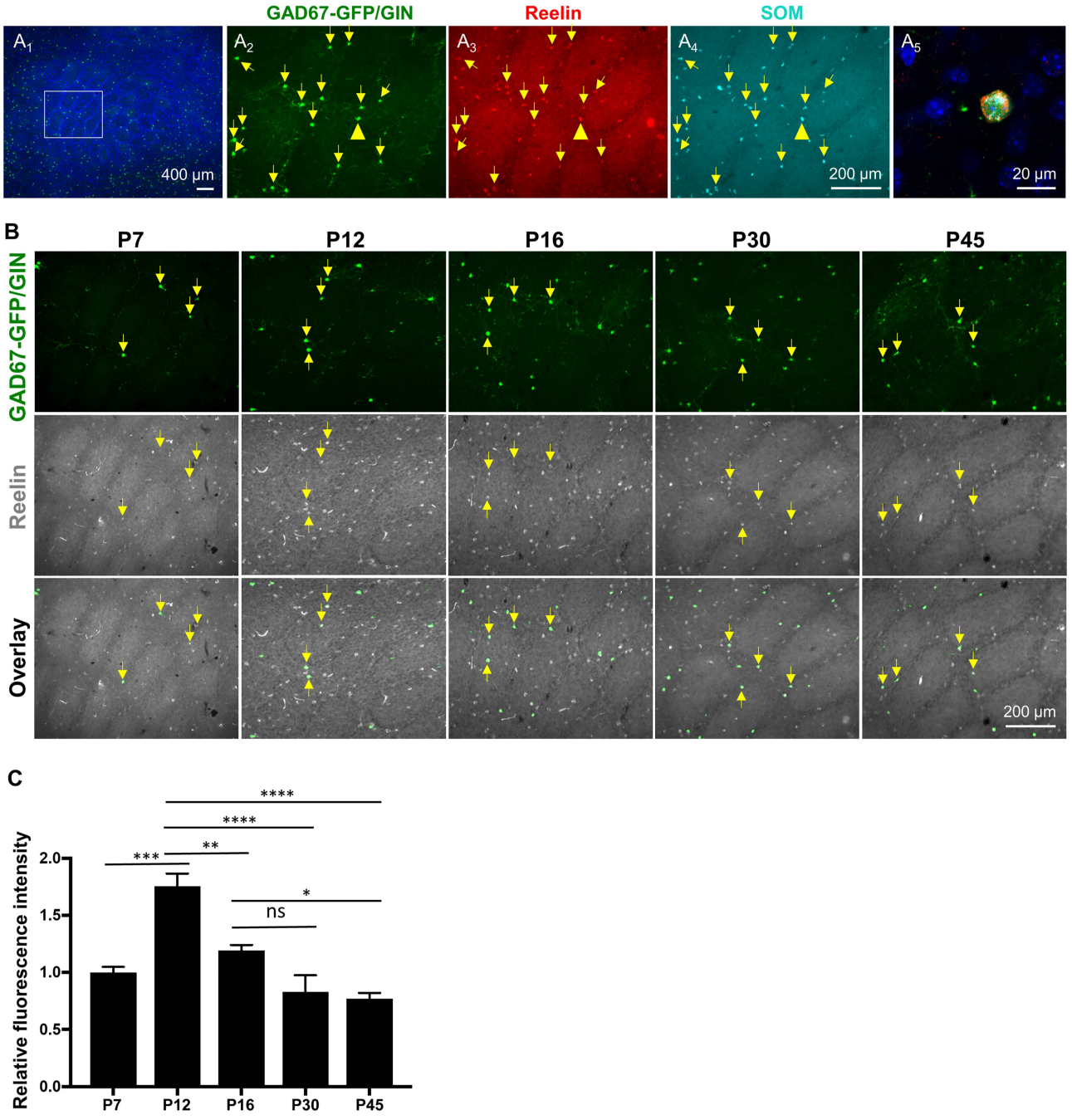

Figure 4. Reelin immunoreactivity in *GAD67-GFP/GIN*-expressing neurons correlates with their morphological maturation in postnatal barrel cortex. (*A*) GFP, Reelin, and SOM triple immunostaining show *GAD67-GFP/GIN*-expressing neurons as a subpopulation of SOM+ neurons expressing Reelin (yellow arrows) in the barrel cortex at P30. (A_1) A low-magnification image with DAPI counterstain of the cell nuclei (blue). (A_2—A_4) Higher magnification images of GFP (green), Reelin (red) and SOM (cyan) staining in the region outlined by a white box in A_1. (A_5) A representative confocal image of colocalization of both Reelin and SOM in a GFP+ neuron indicated by yellow arrowheads in A_2—A_4. (*B*-*C*) Developmental profiling of Reelin immunoreactivity in *GAD67-GFP/GIN*-expressing neurons in the barrel cortex. (*B*) Representative images of double immunostaining of GFP (green) and Reelin (gray) of the PMBSF at indicated ages. (*C*) Fluorescence intensity of Reelin immunostaining in GFP+ neurons at indicated ages normalized to that at P7, indicating a peak of Reelin immunoreactivity in GFP+ neurons at P12. Data represent mean ± SEM, $N = 3$–4 mice per time point, with 10–15 neurons analyzed per mouse. $^{*}P < 0.05$, $^{**}P < 0.01$, $^{***}P < 0.001$, $^{****}P < 0.0001$, and one-way ANOVA followed by Tukey post hoc tests.

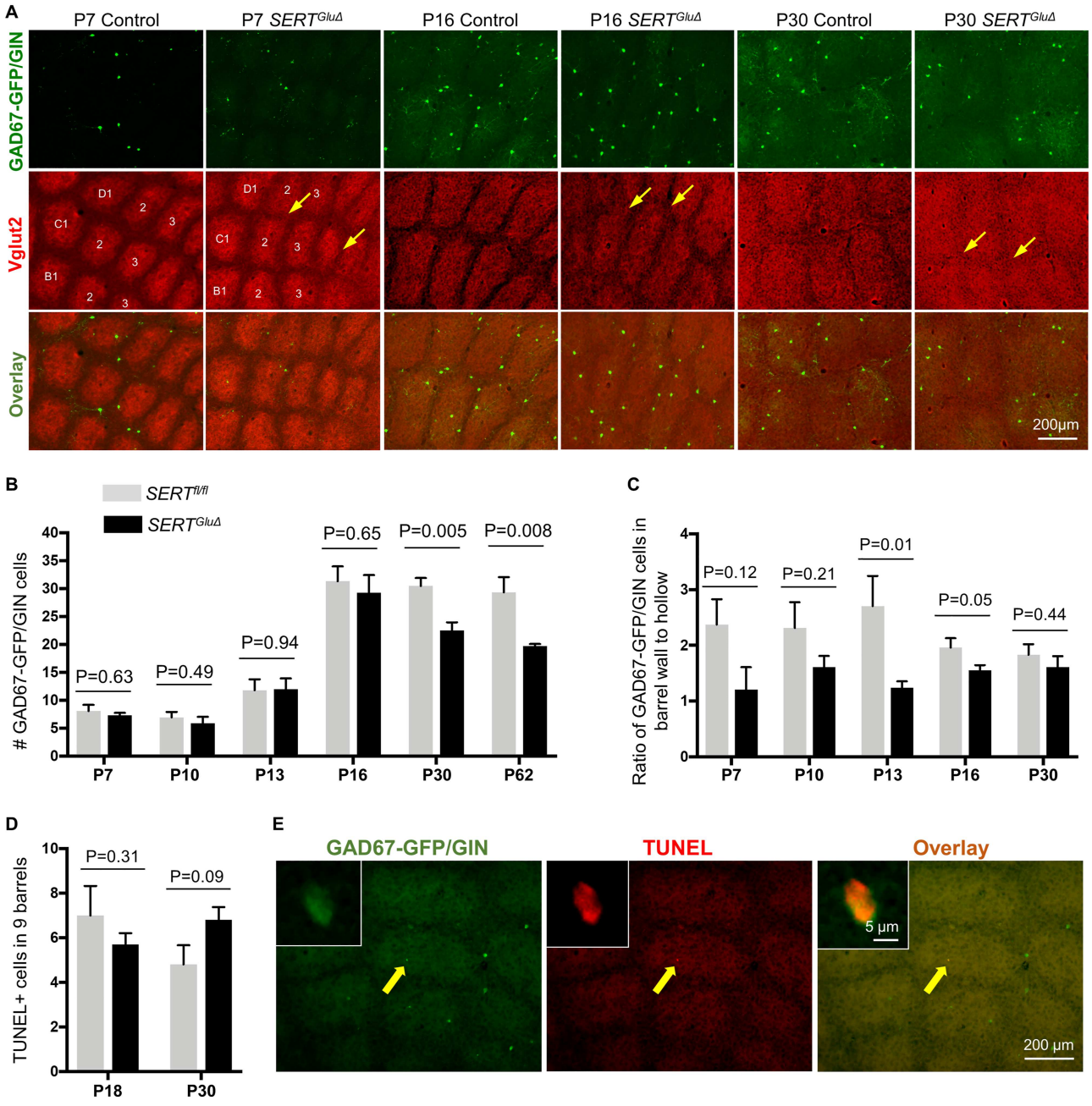

Figure 5. The number and spatial distribution of *GAD67-GFP/GIN*-expressing neurons in the barrel cortex of $SERT^{GluΔ}$ mice. (*A*) Representative images of GFP-expressing neurons in tangential sections of the PMBSF from $SERT^{GluΔ}$ and control littermate mice at indicated ages. Barrels in arcs 1–3 of rows *B-D* are indicated in the P7 cortex. Boundaries between barrels are blurred (arrows) in $SERT^{GluΔ}$ mice at P7 as well as at P16 and P30, while the gross barrel architecture is preserved. (*B-C*) Quantification of the number of GFP+ neurons and their distribution in nine barrels of arcs 1–3 of rows *B-D* of the PMBSF. (*B*) Significant reduction in the number of GFP+ neurons in one- and two-month-old $SERT^{GluΔ}$ mice as compared to control littermates. The numbers of GFP+ neurons at earlier developmental stages were comparable between the two genotypes. (*C*) Evaluation of the spatial distribution of GFP+ neurons in the barrels, by quantifying the ratio of GFP+ neurons in the barrel walls relative to that in the barrel hollows in $SERT^{GluΔ}$ and control mice. For each time point, serial sections through the PMBSF from $SERT^{GluΔ}$ and control littermates were processed and analyzed in parallel. Data represent mean per 50 µm section ± SEM, $N = 4–6$ mice per age per genotype per time point, and *P* values are based on *t*-tests. (*D-E*) Assessing apoptosis by TUNEL assay. (*D*) Quantifying the total number of TUNEL+ cells in arcs 1–3 of rows *B-D* in serial tangential sections through the PMBSF. $N = 5$ mice for each genotype per time point. Data represent mean ± SEM, *t*-tests. (*E*) Representative images showing TUNEL in a GFP+ neuron located in the barrel cortex at P30. Left corner insets show confocal images of the labeled cell indicated by a yellow arrow. The TUNEL+ cell body was smaller, compared to other GFP+ cell bodies in the same brain section, presumably due to shrinking of the dying cell.

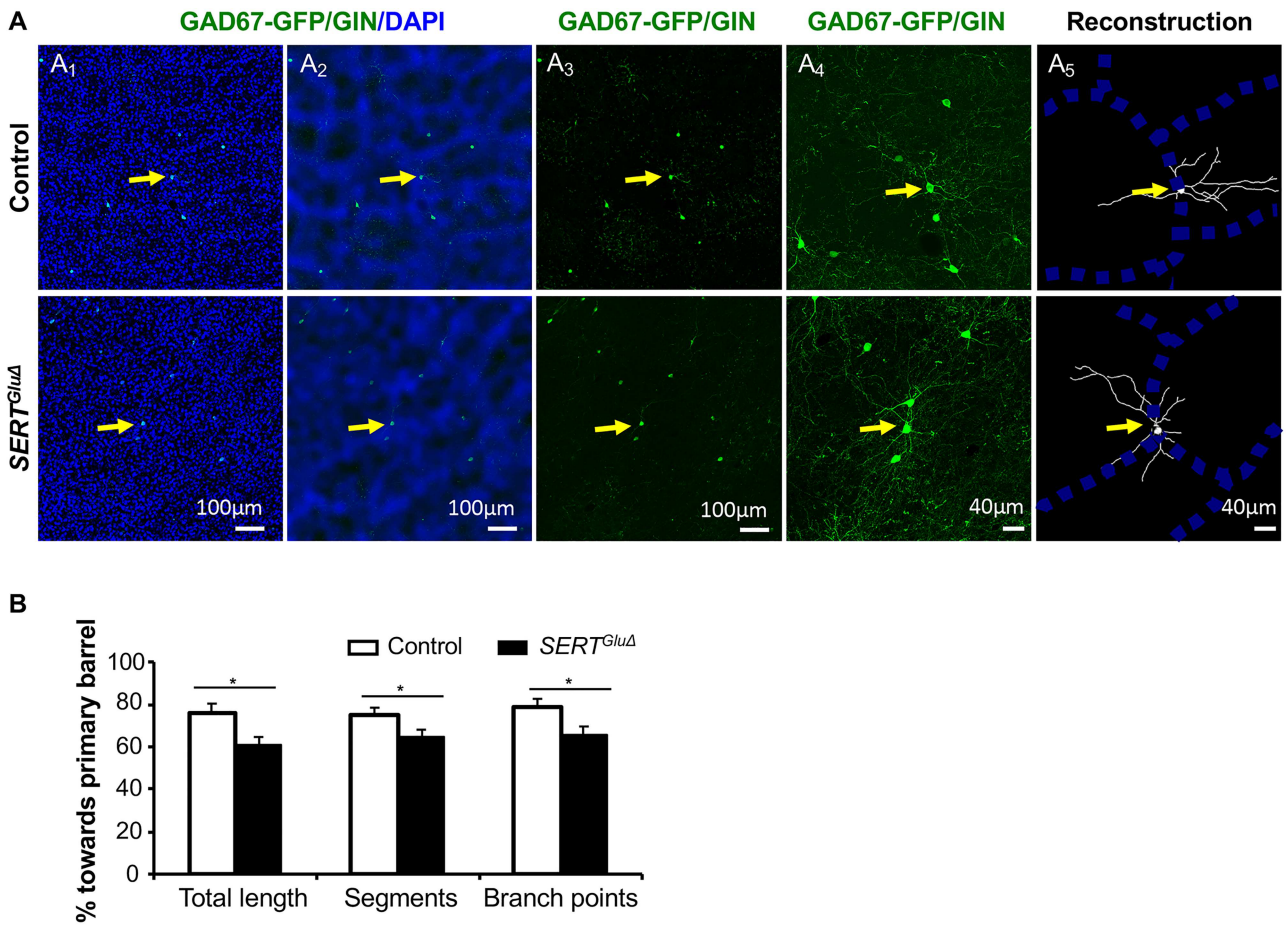

Figure 6. Disrupting SERT expression in developing TCA alters *GAD67-GFP/GIN*-expressing neuron dendrite patterning in the cortex. (*A*) Examples of reconstruction of the dendritic tree of GFP+ neurons located close to the edge of barrel walls in the PMBSF of P30 $SERT^{GluΔ}$ and control littermate mice. (A_1) Low-magnification images showing GFP+ cell bodies (green) at barrel walls delineated by a high density of DAPI-stained cell nuclei (blue) on tangential sections of the PMBSF. (A_2) Original images processed using the mean filter and bandpass filter tools of ImageJ software to define barrel walls. (A_3) GFP+ cells pointed by yellow arrows chosen for reconstruction. (A_4) Higher magnification confocal images of GFP+ dendritic profiles. (A_5) Reconstruction of GFP+ dendritic trees superimposed over barrel walls. (*B*) Quantification of the distribution of the dendrite length, dendritic segments and branching points of GFP+ neurons located at barrel walls relative to corresponding primary barrels in the PMBSF of P30 mice. Each bar represents mean ± SEM, N = 3 mice per genotype, with five neurons analyzed for each $SERT^{GluΔ}$ mouse and 4–6 neurons analyzed for each control mouse, $^*P < 0.05$, *t*-tests.

SERT Expression in Neonatal TCA Determines the Dendrite Patterning of Later Developing Interneurons in the Cortex

SOM-expressing GABAergic neurons are typically wired into a local neuronal network by synaptic connections mostly with nearby glutamatergic neurons (Gentet *et al.* 2012; Sultan *et al.* 2013; Xu *et al.* 2013). During the somatotopic map formation, glutamatergic and GABAergic cortical neurons located in the PMBSF each extend their dendrites predominantly toward dedicated TCA patches that represent sensory information from individual whiskers (Inan and Crair 2007; Espinosa et al. 2009; Chen et al. 2015b). Since *GAD67-GFP/GIN*-expressing neurons grow dendrites after the initial sensory map is established (Figs 1B,C), we asked whether those late-developing neurons that localized to barrel walls also elaborate oriented dendrites, and if deficits in the initial barrel architecture in $SERT^{GluΔ}$ mice would affect dendritic arborization of interneurons that develop late in the cortex.

Because the GFP+ neurons displayed a comparable distribution in the PMBSF of P30 $SERT^{GluΔ}$ and control mice, we characterized dendrite patterning of GFP+ neurons whose cell bodies were located in barrel walls in P30 mice. In control mice, GFP+ neurons located in barrel walls elaborated dendrites primarily targeting to and within a single barrel as outlined by DAPI-labeled cell nuclei, just like the dendrite patterning of cortical neurons established during the initial barrel formation (Inan and Crair 2007; Espinosa *et al.* 2009; Chen *et al.* 2015b), indicating that the dendrites of *GAD67-GFP/GIN*-expressing neurons are integrated into existing barrel architecture. By contrast, in $SERT^{GluΔ}$ mice GFP+ neurons located in barrel walls sent dendrites into multiple adjacent barrels (Fig. 6A). To further characterize the dendritic arborization, we reconstructed the dendritic tree of GFP+ neurons located in barrel walls. We defined a barrel that contains the greatest proportion of dendrite length of a GFP+ neuron as the primary barrel and evaluated oriented dendrite patterning by calculating the distribution of

dendrite length, dendritic segments, and branching points of the neuron with respect to the primary barrel. We found that dendritic length, dendritic segments, and branching points that resided outside primary barrels were all increased for GFP+ neurons in $SERT^{Glu\Delta}$ PMBSF compared to control littermates (Fig. 6B). Despite the dendrite patterning defect, dendritic morphometric parameters such as total dendrite length and the number of branching points were comparable between $SERT^{Glu\Delta}$ and control mice (563.5 ± 65.8 µm vs. 523.8 ± 57.4 µm, $P = 0.65$, and 5.6 ± 0.4 vs. 5.2 ± 0.6, $P = 0.57$, t-test, respectively). Taken together, the results suggest that altered barrel architecture in $SERT^{Glu\Delta}$ mice did not impair the overall dendrite growth and branching complexity of the GFP+ neurons but altered their dendrite patterning.

Discussion

The complexity of cell-autonomous contributions and external influences at target regions pose ample challenges for delineating postnatal neurodevelopmental processes and regulation (Wamsley and Fishell 2017; Lim et al. 2018). Previous studies have investigated interneuron developmental processes through transplantation strategies (Sur and Leamey 2001; Sultan et al. 2013). In this work, we focused our attention to aspects of terminal differentiation features of a population of SOM-expressing GABAergic neurons in their native cortical destination. We demonstrate that a precise cortical architecture at the destination is not essential for those late-developing neurons to acquire and maintain neurochemical specificity, to attain cortical positions, but influences their number ultimately incorporated into the cortical region and their dendrite patterning. Our findings suggest that perturbing the transient early SERT gene function in developing TCA and likely other key components essential for initial cortical map formation represent an origin of the derailment of synaptic architectural trajectory that persists into the adulthood.

Postnatal Development of SOM-Expressing GABAergic Neurons

The protracted period of interneuron development has led to multiple views over genetic programming of cortical maps (Wamsley and Fishell 2017; Lim et al. 2018). By monitoring *GAD67-GFP/GIN*-expressing neurons in the mouse barrel cortex, our study shed some light on processes of terminal specification of a population of SOM-expressing GABAergic neurons. Our BrdU labeling experiments and morphology characterizations indicate that those neurons were born around E13.5 and E14.5 but did not develop mature morphological phenotypes until 2–3 weeks later in the postnatal cortex. As the peak of SOM neuron generation occurs at E12.5 (Bandler et al. 2017), this suggests that those neurons that develop late are also generated relatively late during the neurogenesis of SOM interneurons.

Because cortical neurons are born outside the cortex, one fundamental question has been how postmitotic neurons are assembled into stereotypic cortical maps. Our data indicate that the *GAD67-GFP/GIN*-expressing neurons are integrated into the barrel architecture, by localizing to barrel walls and sending the vast majority of their dendrites into designated TCA patches, just like glutamatergic and GABAergic cortical neurons that assemble into barrels during the initial sensory map formation. However, the processes for patterning cortical neurons during barrel formation and the *GAD67-GFP/GIN*-expressing neurons apparently differ. During barrel formation, the cytoarchitectonic patterning is tightly associated with their oriented dendritic elaboration and coordinated with TCA pattern formation. At birth, cortical neurons of diverse types and TCA from the thalamic VB nuclei are evenly distributed at layer IV of the somatosensory cortex. From P3 to P7, as TCA representing individual whiskers progressively aggregate into patches, connected cortical neurons concurrently localize to the walls (Rebsam et al. 2002; Espinosa et al. 2009). These observations have led to the view that synaptic inputs from TCA drive cortical neurons to barrel walls during initial sensory map establishment (Sur and Leamey 2001; Lim et al. 2018). In contrast, *GAD67-GFP/GIN*-expressing neurons first take residence in barrel walls and then grow their neurites, suggesting that those late-developing neurons can not only be allocated to the barrel cortex but also achieve proper distributions within the barrels, prior to forming specific connections with partners at the terminal positions.

An interesting finding from this work is the expression of Reelin in these late postnatal-developing SOM-expressing neurons. Reelin is an extracellular matrix protein playing multiple important roles in neuronal terminal differentiation (Rakic and Caviness 1995; Ferrer-Ferrer and Dityatev 2018). Temporal-specific Reelin expression has been observed in Cajal-Retzius cells, a special class of pioneer neurons in the embryonic brain (Alcantara et al. 1998). Our data revealed that Reelin is also dynamically regulated in interneurons developing in the late postnatal barrel cortex, with the highest Reelin abundance during the period of their robust neurite outgrowth. Reelin is expressed in GABAergic neurons in many cortical layers and hippocampal subdivisions in the postnatal CNS (Alcantara et al. 1998; Miyoshi et al. 2010; Sohn et al. 2014). Indeed, we found that the majority of Reelin immunolabeled neurons did not express *GAD67-GFP/GIN*. It would be interesting in the future to investigate whether other Reelin-expressing interneurons also develop at late postnatal stages, and the roles of Reelin in developing and mature interneurons.

The Effects of Disrupting Early SERT Function in TCA on Late Postnatal Interneuron Development

Since the transient SERT expression in the TCA governs TCA and cortical neuron patterning during barrel formation and TCA segregation and layer IV neuron patterning are affected in $SERT^{Glu\Delta}$ barrel cortex (Chen et al. 2015b), the changes in *GAD67-GFP/GIN*-expressing neurons in $SERT^{Glu\Delta}$ mice are likely the consequences of deficits resulting from initial barrel formation. An intriguing finding is the reduced number of GFP+ neurons in the barrel cortex in $SERT^{Glu\Delta}$ at P30, even though the numbers were comparable between $SERT^{Glu\Delta}$ mice and control littermate mice up to P16. Although our TUNEL experiments are not conclusive, the data indicate that $SERT^{Glu\Delta}$ did not cause massive cell deaths. Previous studies showed that more than 30% of interneurons generated embryonically are eliminated through programmed cell death postnatally and that the cell death occurs progressively and is linked to circuits assembly (Southwell et al. 2012; Lim et al. 2018). It remains possible that a relatively small increase in neuron apoptosis caused by altered barrel architecture amidst large amounts of intrinsically determined cell death is difficult to discern. We suggest that our findings could be consistent with the idea that initial cortical architecture serves as a template dictating the number of neurons in the adult cortex.

Importantly, although the GFP+ neurons assumed a correct distribution in barrels at P30, they cannot assume oriented dendrite patterning as seen in control mice. The degree of changes in the dendritic patterning of the GFP-expressing neurons is very similar to that of the GABAergic neurons localized to barrel walls during barrel formation in $SERT^{Glu\Delta}$ mice (Chen et al. 2015b). One explanation for this is the existing synaptic architecture shapes connectivity motifs for late-developing neurons. It is also plausible that certain biological processes regulated by SERT function during sensory map formation determine the cues for dendrite patterning of late-developing neurons. Although the precise cause for dendrite patterning defects in $SERT^{Glu\Delta}$ mice remains to be determined, our observations of normal spatial distribution of the GFP-expressing neurons and their defective dendrite patterning in P30 $SERT^{Glu\Delta}$ mice indicate that, unlike during barrel establishment, the spatial organization of those late-developing neurons in the cortex and their dendrite patterning can be regulated and disrupted by distinct mechanisms. Consistent with this idea, expression of the NMDA receptor 2B (NR2B) in the glutamatergic spiny stellate cells is not required for their localization to barrel walls but is essential for the oriented dendritic arborization targeting the primary barrel (Espinosa et al. 2009). Our data suggest that the transient SERT expression in the TCA defines the trajectory of cortical interneuron dendrite patterning in the target sensory cortex.

Recent transcriptome analyses of developing postmortem human brains have implicated that temporal-specific cortical topographic gene expression underscores early-life programming of neural circuits (Geschwind and Rakic 2013; Silbereis et al. 2016). Analyses of developing postmortem brain from individuals affected with autism and fragile X syndrome have revealed that biologically pleiotropic risk genes are clustered in coexpression modules specifically in glutamatergic projection neurons during mid-fetal development (Voineagu et al. 2011; Parikshak et al. 2013; Willsey et al. 2013). Many developmental events in the mid-fetal human brain occur in neonatal mice. Previous studies indicate that circulating 5-HT of gut, placental and maternal origins may penetrate into the developing brain (Bonnin et al. 2007; Cote et al. 2007). Evidence has been mounting that genetic variants reducing SERT gene function or early-life exposure to SERT antagonists increase the risks for developing autism and related traits (Harrington et al. 2013; Glover and Clinton 2016), although SERT antagonists are the first-line treatments of anxiety/depression in adults. Consistently, early-life disruption of SERT gene function has been shown to affect the migration and positioning of cortical interneuron subtypes in mice (Frazer et al. 2015). Our studies illustrate the utility of conditional SERT knockout mice in systematic genetic dissection to reveal not only the biological roles and effects of SERT gene function in the developing and adult CNS, but also where in the brain and in which cells the effects occur and the impact on developmental processes relevant to other neuronal populations.

Supplementary Material

Supplementary material is available at *Cerebral Cortex* online.

Funding

National Institutes of Health (grant MH105839 to J.Y.S.).

Notes

We thank Enpeng Zhao for technical assistance.

References

Alcantara S, Ruiz M, D'Arcangelo G, Ezan F, de Lecea L, Curran T, Sotelo C, Soriano E. 1998. Regional and cellular patterns of reelin mRNA expression in the forebrain of the developing and adult mouse. *J Neurosci*. 18:7779–7799.

Bandler RC, Mayer C, Fishell G. 2017. Cortical interneuron specification: the juncture of genes, time and geometry. *Curr Opin Neurobiol*. 42:17–24.

Bartolini G, Ciceri G, Marin O. 2013. Integration of GABAergic interneurons into cortical cell assemblies: lessons from embryos and adults. *Neuron*. 79:849–864.

Batista-Brito R, Machold R, Klein C, Fishell G. 2008. Gene expression in cortical interneuron precursors is prescient of their mature function. *Cereb Cortex*. 18:2306–2317.

Bonnin A, Torii M, Wang L, Rakic P, Levitt P. 2007. Serotonin modulates the response of embryonic thalamocortical axons to netrin-1. *Nature neuroscience*. 10:588–597.

Chattopadhyaya B, Di Cristo G, Higashiyama H, Knott GW, Kuhlman SJ, Welker E, Huang ZJ. 2004. Experience and activity-dependent maturation of perisomatic GABAergic innervation in primary visual cortex during a postnatal critical period. *J Neurosci*. 24:9598–9611.

Chen JA, Penagarikano O, Belgard TG, Swarup V, Geschwind DH. 2015a. The emerging picture of autism spectrum disorder: genetics and pathology. *Annu Rev Pathol*. 10:111–144.

Chen X, Petit EI, Dobrenis K, Sze JY. 2016. Spatiotemporal SERT expression in cortical map development. *Neurochem Int*. 98:129–137.

Chen X, Ye R, Gargus JJ, Blakely RD, Dobrenis K, Sze JY. 2015b. Disruption of transient serotonin accumulation by non-serotonin-producing neurons impairs cortical map development. *Cell Rep*. 10:346–358.

Cobos I, Calcagnotto ME, Vilaythong AJ, Thwin MT, Noebels JL, Baraban SC, Rubenstein JL. 2005. Mice lacking Dlx1 show subtype-specific loss of interneurons, reduced inhibition and epilepsy. *Nat Neurosci*. 8:1059–1068.

Cossart R. 2011. The maturation of cortical interneuron diversity: how multiple developmental journeys shape the emergence of proper network function. *Curr Opin Neurobiol*. 21:160–168.

Cote F, Fligny C, Bayard E, Launay JM, Gershon MD, Mallet J, Vodjdani G. 2007. Maternal serotonin is crucial for murine embryonic development. *Proceedings of the National Academy of Sciences of the United States of America*. 104:329–334.

de la Torre-Ubieta L, Won H, Stein JL, Geschwind DH. 2016. Advancing the understanding of autism disease mechanisms through genetics. *Nat Med*. 22:345–361.

Denaxa M, Neves G, Rabinowitz A, Kemlo S, Liodis P, Burrone J, Pachnis V. 2018. Modulation of apoptosis controls inhibitory interneuron number in the cortex. *Cell Rep*. 22: 1710–1721.

Deng X, Wang Y, Chou J, Cadet JL. 2001. Methamphetamine causes widespread apoptosis in the mouse brain: evidence from using an improved TUNEL histochemical method. *Brain Res Mol Brain Res*. 93:64–69.

Di G. 2007. Development of cortical GABAergic circuits and its implications for neurodevelopmental disorders. *Clin Genet*. 72:1–8.

Espinosa JS, Wheeler DG, Tsien RW, Luo L. 2009. Uncoupling dendrite growth and patterning: single-cell knockout analysis of NMDA receptor 2B. *Neuron*. 62:205–217.

Ferrer-Ferrer M, Dityatev A. 2018. Shaping synapses by the neural extracellular matrix. *Front Neuroanat*. 12:40.

Frazer S, Otomo K, Dayer A. 2015. Early-life serotonin dysregulation affects the migration and positioning of cortical interneuron subtypes. *Transl Psychiatry*. 5:e644.

Gentet LJ, Kremer Y, Taniguchi H, Huang ZJ, Staiger JF, Petersen CC. 2012. Unique functional properties of somatostatin-expressing GABAergic neurons in mouse barrel cortex. *Nat Neurosci*. 15:607–612.

Geschwind DH, Rakic P. 2013. Cortical evolution: judge the brain by its cover. *Neuron*. 80:633–647.

Glover ME, Clinton SM. 2016. Of rodents and humans: a comparative review of the neurobehavioral effects of early life SSRI exposure in preclinical and clinical research. *Int J Dev Neurosci*. 51:50–72.

Hansson SR, Mezey E, Hoffman BJ. 1998. Serotonin transporter messenger RNA in the developing rat brain: early expression in serotonergic neurons and transient expression in non-serotonergic neurons. *Neuroscience*. 83:1185–1201.

Harrington RA, Lee LC, Crum RM, Zimmerman AW, Hertz-Picciotto I. 2013. Serotonin hypothesis of autism: implications for selective serotonin reuptake inhibitor use during pregnancy. *Autism Res*. 6:149–168.

Inan M, Crair MC. 2007. Development of cortical maps: perspectives from the barrel cortex. *The Neuroscientist*. 13: 49–61.

Lebrand C, Cases O, Adelbrecht C, Doye A, Alvarez C, El S, Seif I, Gaspar P. 1996. Transient uptake and storage of serotonin in developing thalamic neurons. *Neuron*. 17:823–835.

Lebrand C, Cases O, Wehrle R, Blakely RD, Edwards RH, Gaspar P. 1998. Transient developmental expression of monoamine transporters in the rodent forebrain. *J Comp Neurol*. 401:506–524.

Lee FS, Heimer H, Giedd JN, Lein ES, Sestan N, Weinberger DR, Casey BJ. 2014. Mental health. Adolescent mental health–opportunity and obligation. *Science*. 346:547–549.

Lim L, Mi D, Llorca A, Marin O. 2018. Development and functional diversification of cortical interneurons. *Neuron*. 100: 294–313.

Ma Y, Hu H, Berrebi AS, Mathers PH, Agmon A. 2006. Distinct subtypes of somatostatin-containing neocortical interneurons revealed in transgenic mice. *J Neurosci*. 26:5069–5082.

Marin O. 2016. Developmental timing and critical windows for the treatment of psychiatric disorders. *Nat Med*. 22: 1229–1238.

Meyer AH, Katona I, Blatow M, Rozov A, Monyer H. 2002. In vivo labeling of parvalbumin-positive interneurons and analysis of electrical coupling in identified neurons. *J Neurosci*. 22:7055–7064.

Miyoshi G, Hjerling-Leffler J, Karayannis T, Sousa VH, Butt SJ, Battiste J, Johnson JE, Machold RP, Fishell G. 2010. Genetic fate mapping reveals that the caudal ganglionic eminence produces a large and diverse population of superficial cortical interneurons. *J Neurosci*. 30:1582–1594.

Mosley M, Shah C, Morse KA, Miloro SA, Holmes MM, Ahern TH, Forger NG. 2017. Patterns of cell death in the perinatal mouse forebrain. *J Comp Neurol*. 525:47–64.

Narboux-Neme N, Pavone LM, Avallone L, Zhuang X, Gaspar P. 2008. Serotonin transporter transgenic (SERTcre) mouse line reveals developmental targets of serotonin specific reuptake inhibitors (SSRIs). *Neuropharmacology*. 55:994–1005.

Naus CC, Miller FD, Morrison JH, Bloom FE. 1988a. Immunohistochemical and in situ hybridization analysis of the development of the rat somatostatin-containing neocortical neuronal system. *J Comp Neurol*. 269:448–463.

Naus CC, Morrison JH, Bloom FE. 1988b. Development of somatostatin-containing neurons and fibers in the rat hippocampus. *Brain Res*. 468:113–121.

Oliva AA Jr, Jiang M, Lam T, Smith KL, Swann JW. 2000. Novel hippocampal interneuronal subtypes identified using transgenic mice that express green fluorescent protein in GABAergic interneurons. *J Neurosci*. 20:3354–3368.

Parikshak NN, Luo R, Zhang A, Won H, Lowe JK, Chandran V, Horvath S, Geschwind DH. 2013. Integrative functional genomic analyses implicate specific molecular pathways and circuits in autism. *Cell*. 155:1008–1021.

Paul A, Crow M, Raudales R, He M, Gillis J, Huang ZJ. 2017. Transcriptional architecture of synaptic communication delineates GABAergic neuron identity. *Cell*. 171(3):522–539, e520.

Raff MC, Barres BA, Burne JF, Coles HS, Ishizaki Y, Jacobson MD. 1993. Programmed cell death and the control of cell survival: lessons from the nervous system. *Science*. 262:695–700.

Rakic P, Ayoub AE, Breunig JJ, Dominguez MH. 2009. Decision by division: making cortical maps. *Trends Neurosci*. 32:291–301.

Rakic P, Caviness VS Jr. 1995. Cortical development: view from neurological mutants two decades later. *Neuron*. 14:1101–1104.

Rebsam A, Seif I, Gaspar P. 2002. Refinement of thalamocortical arbors and emergence of barrel domains in the primary somatosensory cortex: a study of normal and monoamine oxidase a knock-out mice. *J Neurosci*. 22:8541–8552.

Silbereis JC, Pochareddy S, Zhu Y, Li M, Sestan N. 2016. The cellular and molecular landscapes of the developing human central nervous system. *Neuron*. 89:248–268.

Sohn J, Hioki H, Okamoto S, Kaneko T. 2014. Preprodynorphin-expressing neurons constitute a large subgroup of somatostatin-expressing GABAergic interneurons in the mouse neocortex. *J Comp Neurol*. 522:1506–1526.

Southwell DG, Paredes MF, Galvao RP, Jones DL, Froemke RC, Sebe JY, Alfaro-Cervello C, Tang Y, Garcia-Verdugo JM, Rubenstein JL, et al. 2012. Intrinsically determined cell death of developing cortical interneurons. *Nature*. 491:109–113.

Stiles J, Jernigan TL. 2010. The basics of brain development. *Neuropsychol Rev*. 20:327–348.

Sultan KT, Brown KN, Shi SH. 2013. Production and organization of neocortical interneurons. *Front Cell Neurosci*. 7:221.

Sur M, Leamey CA. 2001. Development and plasticity of cortical areas and networks. *Nat Rev Neurosci*. 2:251–262.

Urban-Ciecko J, Barth AL. 2016. Somatostatin-expressing neurons in cortical networks. *Nat Rev Neurosci*. 17: 401–409.

Voineagu I, Wang X, Johnston P, Lowe JK, Tian Y, Horvath S, Mill J, Cantor RM, Blencowe BJ, Geschwind DH. 2011. Transcriptomic analysis of autistic brain reveals convergent molecular pathology. *Nature*. 474:380–384.

Vong L, Ye C, Yang Z, Choi B, Chua S Jr, Lowell BB. 2011. Leptin action on GABAergic neurons prevents obesity and reduces inhibitory tone to POMC neurons. *Neuron*. 71: 142–154.

Voyvodic JT. 1996. Cell death in cortical development: how much? Why? So what? *Neuron*. 16:693–696.

Wamsley B, Fishell G. 2017. Genetic and activity-dependent mechanisms underlying interneuron diversity. *Nat Rev Neurosci*. 18:299–309.

Willsey AJ, Sanders SJ, Li M, Dong S, Tebbenkamp AT, Muhle RA, Reilly SK, Lin L, Fertuzinhos S, Miller JA, et al. 2013. Coexpression networks implicate human midfetal deep cortical projection neurons in the pathogenesis of autism. *Cell*. 155:997–1007.

Wonders CP, Anderson SA. 2006. The origin and specification of cortical interneurons. *Nat Rev Neurosci*. 7:687–696.

Wong FK, Bercsenyi K, Sreenivasan V, Portales A, Fernandez-Otero M, Marin O. 2018. Pyramidal cell regulation of interneuron survival sculpts cortical networks. *Nature*. 557:668–673.

Xu H, Jeong HY, Tremblay R, Rudy B. 2013. Neocortical somatostatin-expressing GABAergic interneurons disinhibit the thalamorecipient layer 4. *Neuron*. 77:155–167.

Xu X, Roby KD, Callaway EM. 2006. Mouse cortical inhibitory neuron type that coexpresses somatostatin and calretinin. *J Comp Neurol*. 499:144–160.

Xu X, Roby KD, Callaway EM. 2010. Immunochemical characterization of inhibitory mouse cortical neurons: three chemically distinct classes of inhibitory cells. *J Comp Neurol*. 518:389–404.